Microlocal analysis of d-plane transform on the Euclidean space

HIROYUKI CHIHARA
College of Education
University of the Ryukyus

This is a summary of our recently published paper [3] (SIAM J. Math. Anal., 2022). We also mention some supplementary topics and insights. We study the basic properties of d-plane transform on the Euclidean space as a Fourier integral operator, and its application to the microlocal analysis of streaking artifacts in its filtered back-projection. The d-plane transform is defined by integrals of functions on the n-dimensional Euclidean space over all the d-dimensional planes, where $0 < d < n$. This maps functions on the Euclidean space to those on the affine Grassmannian $G(d, n)$. This is said to be X-ray transform if $d = 1$ and Radon transform if $d = n - 1$. When $n = 2$ the X-ray transform is thought to be measurements of CT scanners. In this note we present concrete expression of the canonical relation of the d-plane transform and quantitative properties of the filtered back-projection of the product of the images of the d-plane transform. The latter one is related to the metal streaking artifacts of CT images, and some generalization of recent results of Park-Choi-Seo [18] (Comm. Pure Appl. Math., 2017) and Palacios-Uhlmann-Wang [17] (SIAM J. Math. Anal., 2018) for the X-ray transform on the plane.

Acknowledgment. This work was supported by the Research Institute for Mathematical Sciences, an International Joint Usage/Research Center located in Kyoto University. The author would like to thank Atsuhide Ishida and Koichi Kaizuka for organizing and inviting him to this excellent conference.

1 d-plane transform, back-projections, CT, and artifacts

This note is based on the basic theory of microlocal analysis. See Hörmander's four volumes of textbooks [11], [12], [13], [14], and the textbooks [4] and [7] on Fourier integral operators. In this section we introduce the d-plane transform on the n-dimensional Euclidean space, and review the basic facts about CT scanners.

1.1 d-plane transform and inversion formula

Let $n = 2, 3, 4, \ldots$, and let $d = 1, \ldots, n-1$. We denote by $G_{d,n}$ the Grassmannian which is the set of all d-dimensional vector subspaces of $\mathbb{R}^n$. It is well-known that $\dim G_{d,n} = d(n-d)$. The affine Grassmannian is the set of all d-dimensional planes in $\mathbb{R}^n$, that is,

$$G(d,n) = \{x'' + \sigma \ : \ \sigma \in G_{d,n}, x'' \in \sigma^{\perp}\},$$

where $\sigma^{\perp}$ is the orthogonal complement of σ in $\mathbb{R}^n$. Set

$$N(d,n) := \dim G(d,n) = (d+1)(n-d)$$

for short. We use notation $x'' + \sigma = (\sigma, x'')$.

We fix arbitrary $\sigma \in G_{d,n}$, and divide $x \in \mathbb{R}^n$ as $x = x' + x'' \in \sigma \oplus \sigma^\perp = \mathbb{R}^n$. The d-plane transform of a function $f(x) = f(x' + x'') = \mathcal{O}(\langle x \rangle^{-d-\varepsilon})$ is defined by

$$\mathcal{R}_d f(\sigma, x'') := \int_{x''+\sigma} f = \int_\sigma f(x' + x'') dx', \tag{1}$$

where $\langle x \rangle = \sqrt{1 + |x|^2}$ and dx' is the Lebesgue measure on σ. In particular $\mathcal{R}_1 f$ is called the **X-ray transform** of f, and $\mathcal{R}_{n-1} f$ is called the **Radon transform** of f.

Next we explain the inversion formula of $\mathcal{R}_d$. Roughly speaking, the formal adjoint of $\mathcal{R}_d$ is given as integrals of functions over the set of all d-planes passing through arbitrary fixed point $x \in \mathbb{R}^n$. More precisely

$$\begin{aligned} \mathcal{R}_d^* \varphi(x) &:= \frac{1}{C(d,n)} \int_{\{\Xi \in G(d,n) : x \in \Xi\}} \varphi(\Xi) d\mu(\Xi) \\ &= \frac{1}{C(d,n)} \int_{O(n)} \varphi(x + k \cdot \sigma) dk, \end{aligned}$$

where $\varphi \in C\big(G(d,n)\big)$, $C\big(G(d,n)\big)$ is the set of all continuous functions on $G(d,n)$, $C(d,n) = (4\pi)^{d/2} \Gamma(n/2) / \Gamma\big((n-1)/2\big)$, $\Gamma(\cdot)$ is the gamma function, $O(n)$ is the orthogonal group, $d\mu$ and dk are the normalized measures which are invariant under rotations, and $\sigma \in G_{d,n}$ is arbitrary. The inversion formula of $\mathcal{R}_d$ is given as follows.

Proposition 1 ([10, Theorem 6.2]). *For $f(x) = \mathcal{O}(\langle x \rangle^{-d-\varepsilon})$*

$$f = (-\Delta_x)^{d/2} \mathcal{R}_d^* \mathcal{R}_d f = \mathcal{R}_d^* (-\Delta_{x''})^{d/2} \mathcal{R}_d f,$$

where $-\Delta_x = -\partial_{x_1}^2 - \cdots - \partial_{x_n}^2$ and $-\Delta_{x''}$ is the Laplacian on $\sigma^\perp$.

Operators $\mathcal{R}_d^*$ and $(-\Delta_x)^{d/2} \mathcal{R}_d^* = \mathcal{R}_d^* (-\Delta_{x''})^{d/2}$ are said to be the unfiltered back-projection operator and the filtered back-projection operator respectively.

1.2 CT scanners

We consider two-dimensional CT scanners for cross-sections, and explain that the X-ray transform is considered to be the measurement of CT scanners. In this subsection we assume that the X-ray beam has no width, and traverses the object along a line, say γ below. Let $(x, y) \in \mathbb{R}^2$, and let $f(x, y)$ be a compactly supported function describing the attenuation coefficient distribution of the section of an object. We denote by I_0 and by I the intensities of the beam before and after passing through the object respectively.

Case 1. Uniform media If the object is uniform, that is, $f = a \cdot \chi_\Omega$, where $a \in \mathbb{R}$ is a constant and χ_Ω is the characteristic function of a bounded domain Ω. We denote by ℓ the travel length in the object.

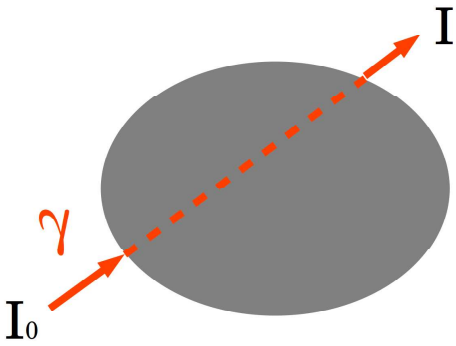

Figure 1. X-ray beam passing though uniform media

Then the Beer-Lambert law obtains

$$\log\left(\frac{I_0}{I}\right) = a \cdot \ell = \int_\gamma f = \mathcal{R}_1 f(\gamma). \tag{2}$$

Case 2. General media Consider the case of Figure 3.

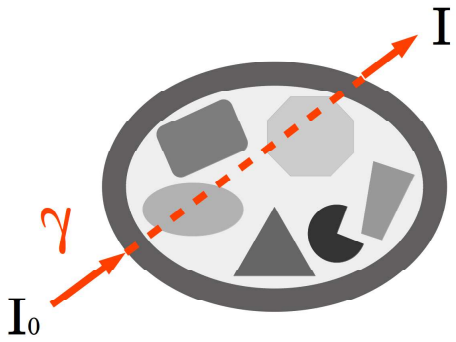

Figure 3. X-ray beam passing though an object

More precisely, f is a compactly supported step function on $\mathbb{R}^2$, and its support is convex. Then $\operatorname{supp} f \cap \gamma$ becomes a line segment. In this case the restriction of $f(x, y)$ on γ is a one-dimensional step function

$$f|_\gamma = \sum_{k=1}^{K} a_k \chi_{\gamma_k},$$

where a_k is a non-zero constant, and γ_k is the k-th line segment of γ in $\operatorname{supp} f$. We denote by I_{k-1} and by I_k the intensities of the beam before and after passing through γ_k. Then $I_K = I$. Repeating the argument of Case 1 above, we deduce that

$$\mathcal{R}_1 f(\gamma) = \int_\gamma f = \sum_{k=1}^{K} \int_{\gamma_k} f = \sum_{k=1}^{K} \log\left(\frac{I_{k-1}}{I_k}\right) = \log\left(\frac{I_0}{I_1} \cdot \frac{I_1}{I_2} \cdots \frac{I_{K-1}}{I}\right) = \log\left(\frac{I_0}{I}\right),$$

which is the same as (2). In this case f and $\mathcal{R}_1 f(\gamma)$ can be also considered to be an approximating step function of some function F and the Riemann sum of $F|_\gamma$ respectively. So we can obtain (2) for more general appropriate functions by the limit process.

We observe an artificial example of a grayscale image of a cross section, its X-ray transform, the unfiltered back-projection, and the filtered back-projection by using the Julia Programming

Language. We introduce the standard coordinates of $G(1,2)$. For arbitrary line $\gamma \in G(1,2)$ in $\mathbb{R}^2$, there exists a pair $(\theta, t) \in [0, 2\pi) \times \mathbb{R}$ such that

$$\begin{aligned}\gamma = L(\theta, t) &= \{(x,y) \in \mathbb{R}^2 \mid x\cos\theta + y\sin\theta = t\} \\ &= \{(x,y) \in \mathbb{R}^2 \mid \cos\theta(x - t\cos\theta) + \sin\theta(y - t\sin\theta) = 0\} \\ &= \{(t\cos\theta - s\sin\theta, t\sin\theta + s\cos\theta) \mid s \in \mathbb{R}\}.\end{aligned}$$

See Figure 4 below. We remark that $L(\theta, t) = L(\theta \pm \pi, -t)$ and $[0, 2\pi) \times \mathbb{R}$ is a double covering of $G(1,2)$.

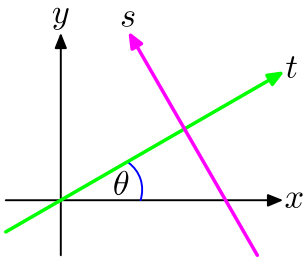

Figure 4. Parametrization (θ, t) of the space $G(1,2)$ of all the lines in $\mathbb{R}^2$

For an appropriate function $f(x,y)$, the X-ray transform $\mathcal{R}_1 f(\gamma)$ is given by

$$\mathcal{R}_1 f(\gamma) = \mathcal{R}_1 f(\theta, t) := \int_\gamma f = \int_{-\infty}^{\infty} f(t\cos\theta - s\sin\theta, t\sin\theta + s\cos\theta) ds.$$

Then we have $\mathcal{R}_1(\theta, t) = \mathcal{R}_1 f(\theta \pm \pi, -t)$. We have only to consider the coordinates $(\theta, t) \in [0, \pi) \times \mathbb{R}$. Here is an artificial example of the set of four grayscale images.

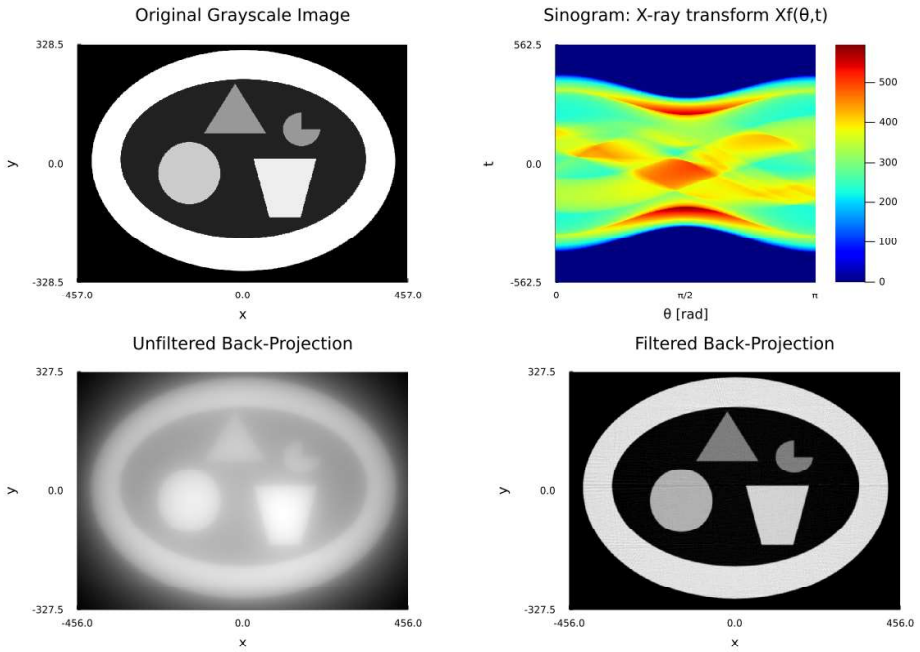

Figure 5. An original gray scale image, its X-ray transform, the unfiltered back-projection, and the filtered back-projection

Here we explain how to see these images.

- **Northwest** A grayscale image is a matrix whose entries are real numbers belonging to the closed interval $[0, 1]$. An element with value 0 expresses a black pixel, an element with value 1 expresses a white pixel, and an element with intermediate value between 0 and 1 expresses an pixel with corresponding gray color.

- **Northeast** This is the heat map of $\mathcal{R}_1 f(\theta, t)$, that is, the value of each entry of the "matrix" $\mathcal{R}_1 f$ is expressed by the sequential color scale indicated in the color bar. The heat map of X-ray transform is called a sinogram.

- **Southwest** This is the unfiltered back-projection $\mathcal{R}_1^* \mathcal{R}_1 f$. More precisely, this is the grayscale image given by a matrix with modified entries defined by

$$\frac{\mathcal{R}_1^* \mathcal{R}_1 f - \min \mathcal{R}_1^* \mathcal{R}_1 f}{\max \mathcal{R}_1^* \mathcal{R}_1 f - \min \mathcal{R}_1^* \mathcal{R}_1 f},$$

  whose entries are in the interval $[0, 1]$. The grayscale image of $\mathcal{R}_1^* \mathcal{R}_1 f$ is blurred.

- **Southeast** This is the filtered back-projection $(-\partial_x^2 - \partial_y^2)^{1/2} \mathcal{R}_1^* \mathcal{R}_1 f$. Roughly speaking, the first derivative of the unfiltered back-projection is clear and gives the reconstruction of f from the measurement $\mathcal{R}_1 f$. The relationship between unfiltered and filtered back-projections is similar to that of the rectified linear unit (ReLU) and the Heaviside function on $\mathbb{R}$. If we set

$$\mathrm{ReLU}(s) = \begin{cases} s & (s > 0), \\ 0 & (s < 0), \end{cases} \quad Y(s) = \begin{cases} 1 & (s > 0), \\ 0 & (s < 0), \end{cases}$$

  then we have

$$\frac{d}{ds}\mathrm{ReLU} = Y$$

  in the sense of distribution. The Heaviside function $Y(s)$ describes the step difference at $s = 0$ clearly, and the ReLU does not.

It might be somewhat difficult to understand the correspondence of the original grayscale image and the sinogram. So the author opens computer program based notebooks illustrating this correspondence at the **GitHub** page

`https://github.com/hiroyuki-chihara/xray`

which is clickable in the PDF of this manuscript. The author provides two notebooks there.

- A notebook created by **Pluto.jl** of **Julia Programming Language**.

- A notebook created by **Live Script** of **MATLAB**.

1.3 Metal streaking artifacts

There are some factors causing artifacts in CT images: beam width, partial volume effect, beam hardening, noise in measurements, numerical errors, and etc. See, e.g., Epstein's celebrated textbook on medical imaging [5]. In this note we study the beam hardening effect causing metal streaking artifacts. It is known that this phenomenon occurs for the CT images of human bodies containing metal regions such as implants, stents, metal bones and etc.

In the formulation of (2), the X-ray is supposed to be monochromatic with a fixed energy, say $E_0 > 0$. Actually, however, the X-ray beam has a wide range of energy $E \in [0, \infty)$, and the attenuation coefficient distribution f_E depends on E. This is described by the spectral function $\rho(E)$ which is a probability density function of $E \in [0, \infty)$. In this case the formulation of the measurements P of CT scanners becomes

$$P := \log\left(\frac{I_0}{I}\right) = -\log\left\{\int_0^\infty \rho(E)\exp(-\mathcal{R}_1 f_E)dE\right\}.$$

If f_E is independent of E, i.e., $f_E = f_{E_0}$, then

$$\begin{aligned}\log\left(\frac{I_0}{I}\right) &= -\log\left\{\int_0^\infty \rho(E)dE \cdot \exp(-\mathcal{R}_1 f_{E_0})\right\} \\ &= -\log\big\{\exp(-\mathcal{R}_1 f_{E_0})\big\} = \mathcal{R}_1 f_{E_0}.\end{aligned}$$

Recently, the beam hardening effect and metal streaking artifacts were studied from the viewpoint of microlocal analysis. Let D be a metal region in $\mathbb{R}^2$. Consider a simple model of spectral function and beam hardening effect of the form

$$\begin{aligned}\rho(E) &= \frac{1}{2\varepsilon}\chi_{[E_0-\varepsilon, E_0+\varepsilon]}(E), \\ f_E(x) &= f_{E_0}(x) + \alpha(E - E_0)\chi_D(x),\end{aligned}$$

where f_{E_0} is an attenuation coefficient distribution of normal human tissue, ε and α are small positive constants, and D is a metal region which is a disjoint union of finitely many strictly convex bounded domains with smooth boundaries. Then the measurement P becomes

$$P - \mathcal{R}_1 f_{E_0} = -\log\left\{\frac{\sinh(\alpha\varepsilon\mathcal{R}_1\chi_D)}{\alpha\varepsilon\mathcal{R}_1\chi_D}\right\} = \sum_{k=1}^{\infty} A_k(\alpha\varepsilon\mathcal{R}_1\chi_D)^{2k}.$$

This means that P consists of the normal tissue part and the beam hardening part, and that the latter part is a (formal) power series of $\big(\mathcal{R}_1\chi_D\big)^2$. The main object is the filtered back-projection of the power series. Here are pioneering works on the microlocal analysis of metal streaking artifacts for this simple model.

- Park, Choi, and Seo ([18] Comm. Pure Appl. Math., 2017) proved that the metal streaking artifacts are propagation of $\mathrm{WF}(\chi_D)$ along the union of the common tangential lines $\mathcal{L}$ of metal domains.

- Palacios, Uhlmann, and Wang ([17] SIAM J. Math. Anal., 2018) proved that the streaking artifacts are conormal distributions supported by $\mathcal{L}$.

The following figure illustrates a grayscale image of two disks of metal regions with different radii, its X-ray transform, the filtered back-projection, and the filtered back projection of $\left(\mathcal{R}_1\chi_D\right)^2$, which is the principal part of the beam hardening effect. The southeast image illustrates the streaking artifacts of four common tangential lines of the two disks.

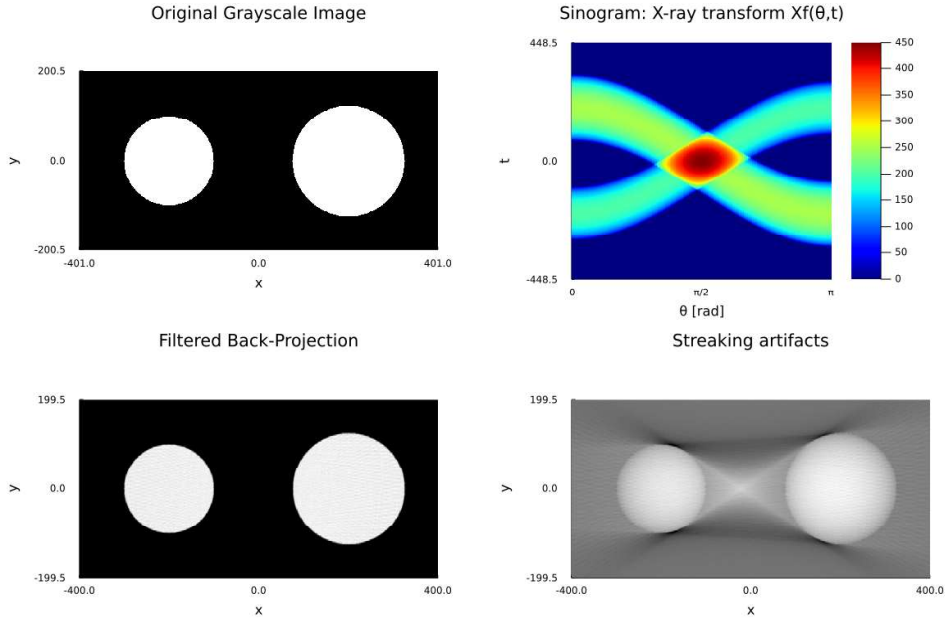

Figure 6. Two disks, the sinogram, the standard FBP, and the FBP of $\left(\mathcal{R}_1\chi_D\right)^2$.

In this note we study the higher dimensional generalization of [17].

2 Conormal distributions

Comparing unfiltered and filtered back projections, one can understand that singularities are the essential part of information contained in imaging data. In this note we quantitatively deal with generalized functions or the distribution kernels of linear operators. So we use the classifications of Schwartz distributions based on singular supports, singular directions, and the order of singularities. These are called the classes of Lagrangian distributions. This section provides preliminaries. we mainly pick up conormal distributions, which are simple examples of Lagrangian distributions.

Definition 2 (Conormal distributions)**.** Let X be an N-dim manifold, and let Y be a closed submanifold of X. A Schwartz distribution $u \in \mathscr{D}'(X)$ is said to be conormal with respect to Y of degree m if

$$L_1 \cdots L_M u \in {}^{\infty}H^{\mathrm{loc}}_{(-m-N/4)}(X)$$

for all $M = 0, 1, 2, \ldots$ and all vector fields $L_1, \ldots, L_M$ tangential to Y. Denote by $I^m(X; N^*Y)$, the set of all distributions on X conormal with respect to Y of degree m.

Note that $N^*_y Y := T^*_y X / T^*_y Y$ for any $y \in Y$, and

$$\|u\|_{{}^{\infty}H_{(s)}(\mathbb{R}^N)} := \sup_{j=0,1,2,\ldots} \left(\int_{A_j} \langle \xi \rangle^{2s} |\hat{u}(\xi)|^2 d\xi \right)^{1/2},$$

$$A_0 := \{|\xi| < 1\}, \quad A_j := \{2^{j-1} \leqq |\xi| < 2^j\}, j = 1, 2, 3, \dots .$$

Roughly speaking, a conormal distribution $u \in I^m(X; N^*Y)$ is a distribution on X such that $u \in C^\infty(X \backslash Y)$, that is, $\operatorname{singsupp} u \subset Y$, and the microlocal singularities of u on Y are limited to the normal directions of Y. If $u \in I^m(X; N^*Y)$, then $\mathrm{WF}(u) \subset N^*Y \setminus 0$. It is very interesting that conormal distributions can be characterized by oscillatory integrals locally.

Proposition 3 ([13, Theorem 18.2.8]). *Let $x = (x', x'') \in \mathbb{R}^k \times \mathbb{R}^{N-k}$ and let $Y = \{0\} \times \mathbb{R}^{N-k} = \{x' = 0\}$. Then $u \in \mathscr{D}'(\mathbb{R}^N)$ belongs to $I^{m+k/2-N/4}(\mathbb{R}^N; N^*Y)$ if and only if there exists an amplitude $a(x'', \xi') \in S^m(\mathbb{R}^{N-k} \times \mathbb{R}^k)$ such that*

$$u(x) = \int_{\mathbb{R}^k} e^{ix' \cdot \xi'} a(x'', \xi') d\xi'.$$

Here $S^m(\mathbb{R}^{N-k} \times \mathbb{R}^k)$ is the standard symbol class, that is, we say that a smooth function $a(x'', \xi')$ belongs to $S^m(\mathbb{R}^{N-k} \times \mathbb{R}^k)$ if for any compact set $K \subset \mathbb{R}^{N-k}$ and for any multi-indices α' and β'', there exists a constant $C(K, \alpha, \beta) > 0$ such that

$$|\partial_{x''}^{\beta''} \partial_{\xi'}^{\alpha'} a(x'', \xi')| \leqq C(K, \alpha, \beta) \langle \xi' \rangle^{m - |\alpha'|}, \quad (x'', \xi') \in K \times \mathbb{R}^k.$$

We can replace the conormal bundle N^*Y by more general conic Lagrangian submanifold Λ. The elements of $I^m(X; \Lambda)$ is said to be Lagrangian distributions on X. These are characterized as oscillatory integrals with more general phase functions of the form:

$$u(x) = \int e^{i\phi(x,\theta)} a(x, \theta) d\theta.$$

The distributions kernels of Fourier integral operators are Lagrangian distributions.

We now see typical examples of conormal distributions.

Example 4 (A characteristic funtion of a smooth domain). *If D be a domain in $\mathbb{R}^n$ with smooth boundary, then the characteristic function χ_D of D belongs to $I^{-1/2-n/4}\big(\mathbb{R}^n; N^*\partial D\big)$.*

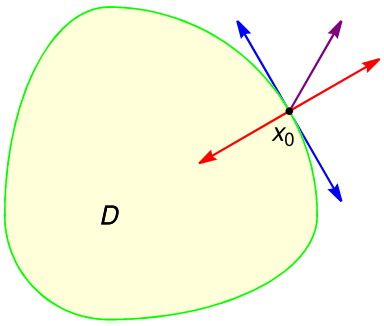

Figure 7. A bounded domain with smooth boundary, and smooth and singular directions

Example 5 (The distribution kernal of a pseudodifferential operator). *Set*

$$\Delta = \{(x, x) : x \in \mathbb{R}^N\},$$

which is the diagonal part of $\mathbb{R}^N \times \mathbb{R}^N$. If $a(x, \xi) \in S^m(\mathbb{R}^N \times \mathbb{R}^N)$, then

$$K(x, y) = \int_{\mathbb{R}^N} e^{i(x-y)\cdot\xi} a(x, \xi) d\xi \in I^m(\mathbb{R}^N \times \mathbb{R}^N; N^*\Delta),$$

$$N^*\Delta = \{(x, x; \xi, -\xi) : x, \xi \in \mathbb{R}^N\}.$$

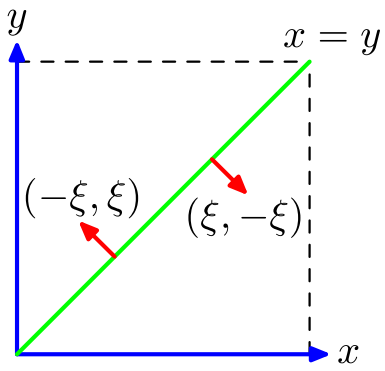

Figure 8. The singular support of the distribution kernel of a pseudodifferential operator

3 Canonical relation of d-plane transform

The canonical relation of a Fourier integral operator describes the mapping properties of microlocal singularities before and after the operator applies to a function. In this note the canonical relation of the d-plane transform plays a crucial role in our microlocal analysis. It is well-known the canonical relation of the X-ray transform $\mathcal{R}_1$ on the plane $\mathbb{R}^2$. See [19] or [15] for this. Moreover, this has been often used for applied mathematics related to medical imaging. Andrade-Loarca et al [1] constructed their original deep neural network detecting the wave front sets of distributions of two variables and detected the wave front set of sinograms by using the canonical relations. Bubba et al [2] used this canonical relation and designed their own deep neural network reconstructing CT images from limited CT data. However, for the other cases $(d, n) \neq (1, 2)$, we could not find the concrete expression of the canonical relation of the d-plane transform. So we tried to compute this by ourselves.

Theoretically, it is known that the incidence relation obtains the canonical relations of integral transforms such as d-plane transform. See [8] and [20]. However, it is not so easy to compute the conormal bundle of a subset of $G(d, n) \times \mathbb{R}^n$ in the cotangent bundle $T^*\big(G(d, n) \times \mathbb{R}^n\big)$. So we establish the generalized Fourier slice theorem for d-plane transform, and obtain the concrete expression of the distribution kernel $K\big((\sigma, x''), y\big)$ of the d-plane transform:

$$K\big((\sigma, x''), y\big) = \frac{1}{(2\pi)^{n-d}} \int_{\sigma^\perp} e^{i(x''-y)\cdot\xi} d\xi, \quad \big((\sigma, x''), y\big) \in G(d, n) \times \mathbb{R}^n. \tag{3}$$

We can compute the canonical relation of the d-plane transform using the phase function

$$\phi\big((\sigma, x''), y; \xi\big) = (x'' - y) \cdot \xi, \quad \big((\sigma, x''), y\big) \in G(d, n) \times \mathbb{R}^n,\ \xi \in \sigma^\perp.$$

Theorem 6. *$\mathcal{R}_d$ is an elliptic Fourier integral operator such that*

$$K\big((\sigma, x''), y\big) \in I^{-d(n-d+1)/4}\big(G(d, n) \times \mathbb{R}^n; \Lambda_\phi\big),$$

$$\begin{aligned}\Lambda'_\phi = \big\{\big(\sigma, y - \pi_\sigma y, y;\ \eta(y \cdot \omega_1, \ldots, y \cdot \omega_d, 1, 1)\big) :\\ \sigma = \langle \omega_1, \ldots, \omega_d \rangle \in G_{d,n},\ \omega_1, \ldots, \omega_d \in \mathbb{S}^{n-1},\ y \in \mathbb{R}^n,\ \eta \in \sigma^\perp\big\}\end{aligned}$$

$$= \big\{ \big(\sigma, x'', x'' + t_1\omega_1 + \cdots + t_d\omega_d;\ \xi(t_1, \ldots, t_d, 1, 1)\big) : \\ (\sigma, x'') \in G(d,n),\ \sigma = \langle \omega_1, \ldots, \omega_d \rangle \in G_{d,n}, \\ \omega_1, \ldots, \omega_d \in \mathbb{S}^{n-1},\ t_1, \ldots, t_d \in \mathbb{R},\ \xi \in \sigma^\perp \big\},$$

where π_σ is the orthogonal projection of $\mathbb{R}^n$ onto $\sigma \in G_{d,n}$.

The most important thing is that all the elements of fiber variables are of the form

$$\text{scalar} \quad \times \quad \text{a common element } \eta \in \sigma^\perp.$$

This fact plays a crucial role when we consider the canonical relation of $\mathcal{R}_d^*$. This means that if microlocal singularities in $G(d,n)$ differ from this form, such singularities never arise in $\mathbb{R}^n$.

Unfortunately, however, it might be difficult to understand the meaning of the frequency part of the canonical relation above. So we consider the canonical relation of the geodesic X-ray transform on an n-dimensional Riemannian manifold (M, g), where g is a Riemannian metric tensor on a smooth manifold M. We denote by $\mathcal{G}$ the set of all the normal geodesics in (M, g). Then $\mathcal{G}$ becomes a $2(n-1)$-dimensional smooth manifold like $G(1,n)$. Indeed, for each hypersurface Σ in M, local coordinates of $\mathcal{G}$ is given by the pair of the passing point on Σ and the direction for the normal geodesics passing through Σ. For an appropriate function f on M, the geodesic X-ray transform of f is defined by

$$\mathcal{X}f(\gamma) := \int_\gamma f = \int f(\exp_p t\omega)dt, \quad \gamma = \exp_p \cdot\omega \in \mathcal{G}$$

with some $(p, \omega) \in S^*M$, where S^*M is the unit cotangent sphere bundle over M. The canonical relation of $\mathcal{X}$ is a conic Lagrangian submanifold of $T^*(\mathcal{G} \times M) \setminus 0$ given by

$$\Lambda' = \{(\gamma_{q,\omega}, q; \eta(t_0), -\Gamma^i_{jk}(p(t_0))\omega_j(t_0)\eta_k(t_0), \eta) : (q,\eta) \in T^*(M) \setminus 0, \omega \in S^*_q(M) \cap \eta^\perp\}$$

where $\gamma_{q,\omega} = \exp_p \cdot\omega$, $p(t) = \gamma_{q,\omega}(t)$, $\omega(t) = \dot\gamma_{q,\omega}(t)$, $\eta(t)$ is the parallel transport of η along $\gamma_{q,\omega}$ at $p(t)$, $t_0 \in \mathbb{R}$ is some constant, and $\Gamma^i_{jk}(p)$ is the Christoffel symbol of the Levi-Civita connection at $p \in M$. The canonical relation Λ' says that the geodesic X-ray transform maps the visible singularity η at point q to the **horizontal lift of the parallel transport** of η along the geodesic flow $(\gamma_{q,\omega}, \dot\gamma_{q,\omega})$.

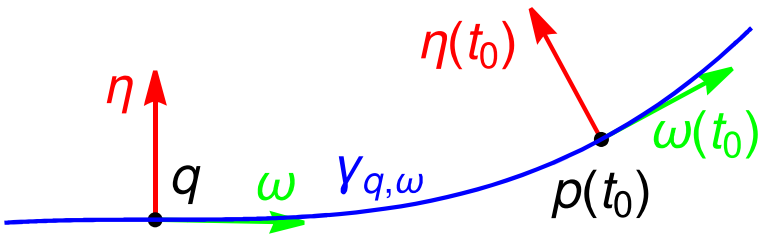

Figure 9. The canonical transform of $T^*M \setminus 0$ to $T^*\mathcal{G} \setminus 0$

The canonical relation of $\mathcal{R}_1$ on $\mathbb{R}^2$ is given by

$$C_1' = \left\{ \left(\theta, t, \begin{bmatrix} t\cos\theta - s\sin\theta \\ t\sin\theta + s\cos\theta \end{bmatrix};\ -\tau s \begin{bmatrix} -\sin\theta \\ \cos\theta \end{bmatrix}, \tau, \tau \begin{bmatrix} \cos\theta \\ \sin\theta \end{bmatrix} \right) : t, s, \tau \in \mathbb{R},\ \theta \in [0, \pi] \right\}$$

$$= \left\{ \left(\frac{\xi}{|\xi|}, \frac{x \cdot \xi}{|\xi|}, x; \mp|\xi| \left(x - \frac{x \cdot \xi}{|\xi|^2} \right) \xi, \pm|\xi|, \xi \right) : (x, \xi) \in T^*\mathbb{R}^2 \setminus 0 \right\}.$$

We have

$$\mathrm{WF}(\mathcal{R}_1 f) = C_1' \circ \mathrm{WF}(f) := \{(p, \xi) : (p, q; \xi, \eta) \in C_1', (q, \eta) \in \mathrm{WF}(f)\}$$

since $\mathcal{R}_1$ on the plane is an elliptic Fourier integral operator. Figure 10 shows a grayscale image of a square, its sinogram, the wave front set of the square in $S^*\mathbb{R}^2$, and the wave front set of the sinogram normalized in some sense.

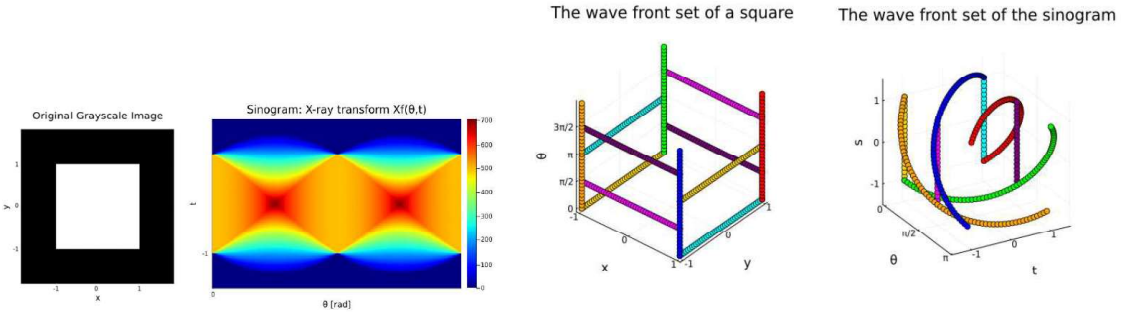

Figure 10. A square, its sinogram, and their wave front sets

4 Main Theorem

In this section we state our main theorem of this note, and explain its meaning using some figures. Firstly we state our assumption about the metal region, and set some notation.

Assumption. The metal region $D \subset \mathbb{R}^n$ is supposed to be a disjoint union of finitely many D_j $(j = 1, \ldots, J)$ which are simply connected, strictly convex, and bounded with smooth boundaries $\Sigma_j := \partial D_j$. Set $\Sigma := \partial D$.

Denote by $\nu(y_j)$ the unit outer normal vector of Σ_j at $y_j \in \Sigma_j$. We consider the set of pairs $(y_j, y_k) \in \Sigma_j \times \Sigma_k$ such as

$$\mathcal{M}_{jk}^{(\pm)} := \{(y_j, y_k) \in \Sigma_j \times \Sigma_k \ : \ y_j + T_{y_j}\Sigma_j = y_k + T_{y_k}\Sigma_k, \ \nu(y_j) = \pm\nu(y_k)\}.$$

We can confirm that this is an $(n-2)$-dimensional submanifold of $\Sigma_j \times \Sigma_k$. Using this we can introduce the set of lines

$$\mathcal{L}_{jk}^{(\pm)} := \{y_j + t(y_k - y_j) \ : \ (y_j, y_k) \in \mathcal{M}_{jk}^{(\pm)}, \ t \in \mathbb{R}\},$$

Then $\mathcal{L}_{jk}^{(\pm)}$ becomes a cylindrical surface or a cone which is tangent to Σ_j at y_j and to Σ_k at y_k for all $(y_j, y_k) \in \mathcal{M}_{jk}^{(\pm)}$. Set $\mathcal{L}_{jk} := \mathcal{L}_{jk}^{(+)} \cup \mathcal{L}_{jk}^{(-)}$ and $\mathcal{L} := \bigcup_{j<k} \mathcal{L}_{jk}$.

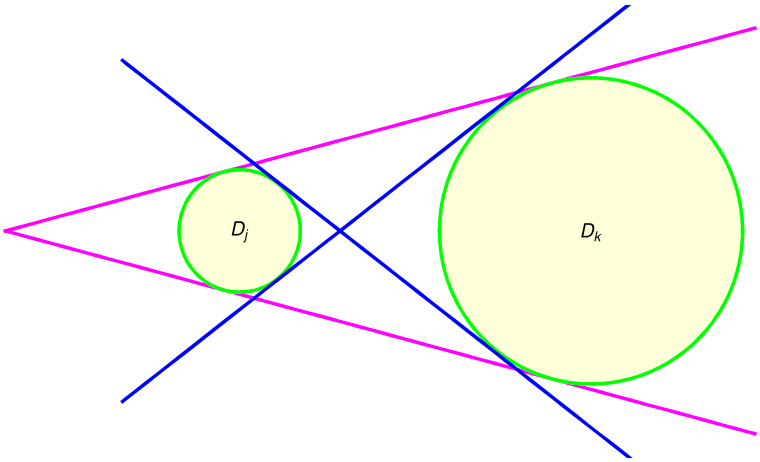

Figure 11. Σ_j, Σ_k, $\mathcal{L}^{(+)}_{jk}$, and $\mathcal{L}^{(-)}_{jk}$

We set the notation for the CT image corresponding to the beam hardening effect as a formal series of the form

$$f_{MA} := f_{CT} - f_{E_0} = \sum_{k=1}^{\infty} A_k (a\varepsilon)^{2k} \mathcal{R}_d^* (-\Delta_{x''})^{d/2} [(\mathcal{R}_d \chi_D)^{2k}],$$

where A_k ($k = 1, 2, 3, \dots$), a, and ε are real-valued constants. We now state our main theorem.

Theorem 7. *Away from* Σ,

$$f_{MA} \in I^{-(d+2+n/4)+d(n-d)/2}(\mathbb{R}^n; N^* \mathscr{L}).$$

The principal symbol of the FBP of $(\mathcal{R}_d \chi_D)^2$ *does not vanish.*

All the known results related to our main theorem are limited to the case $(n, d) = (2, 1)$.

- Park, Choi, and Seo ([18], 2017) proved that $\mathrm{WF}(f_{\mathrm{MA}}) \subset N^* \mathscr{L}$.
- Palacios, Uhlmann, and Wang ([17], 2018) proved Theorem 7.
- Wang and Zou ([21], 2021) studied the studied the case that $D_1, \dots, D_J$ are not necessarily convex. This is difficult setting, and they obtained some results.

We explain what Theorem 7 says.

- If Σ_j and Σ_k have a common tangential hyperplane, then the common conormal singularity propagates all over the line connecting the tangential points. This is the true identity of the metal streaking artifacts.

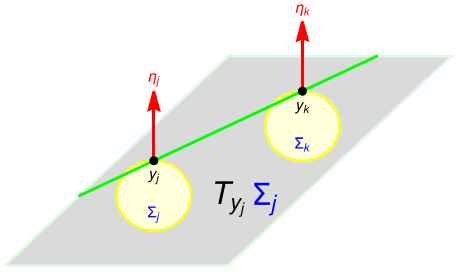

Figure 12. The case that there exists a common hyperplane passing through y_j and y_k for $(y_j, y_k) \in \mathcal{M}^{(\pm)}_{jk}$, that is, $\nu(y_j) = \nu(y_k)$ or $\nu(y_j) = -\nu(y_k)$.

- If Σ_j and Σ_k have a common tangential plane of codimension two, then the normal directions at the tangential points are different and no singularity propagates along the connecting line.

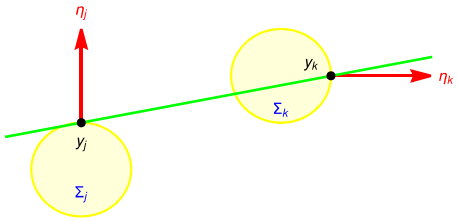

Figure 13. The case that there is not a common hyperplane passing through y_j and y_k for $(y_j, y_k) \in \mathcal{M}_{jk}^{(\pm)}$, that is, $\nu(y_j) \neq \nu(y_k)$ and $\nu(y_j) \neq -\nu(y_k)$.

We consider only smooth boundary Σ. Actually, however, it is possible to consider nonsmooth boundary such as polyhedrons. Indeed Palacios, Uhlmann, and Wang ([17], 2018) studied also the case that some D_j are polygons on the plane. In this case we need to consider the interaction of microlocal singularities arising from edges and vertices. More precisely, there are three types of interaction: edge-edge, vertex-vertex, and edge-vertex. In particular we remark that all the directions are singular directions at vertices. We can observe edge-edge and vertex-vertex interactions in the next figure.

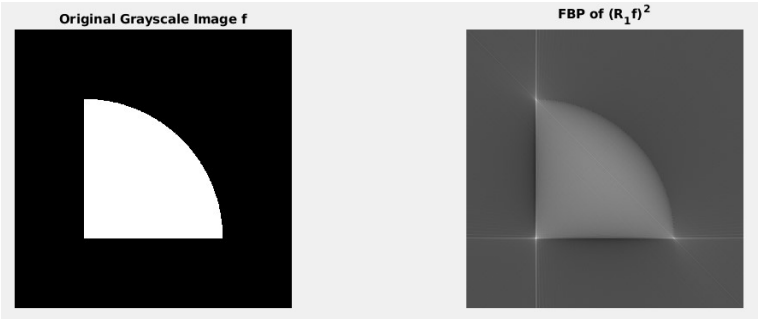

Figure 14. Edge-edge and vertex-vertex interactions

We can consider the case that some D_j are convex polyhedrons in $\mathbb{R}^3$. Unfortunately, however, I gave up this trial since we needed to consider many types of interaction such as vertex-vertex, vertex-edge, vertex-face, edge-edge, edge-face, and face-face.

5 Proof of Theorem 7

Finally we explain the outline of the proof of Theorem 7. The main part of the proof is the evaluation of the product of Lagrangian distributions $\mathcal{R}_{d\chi_{D_j}}$, and relies on advanced theory of microlocal analysis such as paired Lagrangian distributions, which was developed in Melrose and Uhlmann [16], and Greenleaf and Uhlmann [6]. So we need so-called the intersection calculus of manifolds. We split this section into three subsections: intersection calculus, paired Lagrangian distributions, and overview of the proof.

5.1 Intersection calculus for $\mathcal{R}_{d\chi_{D_j}}$

We state the definition of transversal intersection and clean intersection.

Definition 8. Let X be a smooth manifold, and let Y and Z be submanifolds of X.

- We say that Y and Z intersect transversely if $N^*_xY \cap N^*_xZ = \{0\}$ for all $x \in Y \cap Z$. Note that this condition is equivalent to that $T_xY \cup T_xZ = T_xX$ for all $x \in Y \cap Z$.
- We say that Y and Z intersect cleanly if $Y \cap Z$ is smooth and $T_xY \cap T_xZ = T_x(Y \cap Z)$ for all $x \in Y \cap Z$. Moreover,

$$e := \operatorname{codim}(Y) + \operatorname{codim}(Z) - \operatorname{codim}(Y \cap Z)$$

  is said to be the excess of the intersection.

We remark that transverse intersection is clean intersection with no excess. Here we observe two examples of intersections of two surfaces in xyz-space $\mathbb{R}^3$. We set

$$Y_1 = \{z = x + y\}, \quad Y_3 = \{z = (x + y)^3\}, \quad Z = \{z = 0\}.$$

Then $Y_k \cap Z = \{(x, -x, 0)\}$. For any $p \in Y_k \cap Z$ we have

$$\begin{aligned} T_p(Y_k \cap Z) &= T_pY_1 \cap T_pZ = \langle (1, -1, 0) \rangle_{\mathbb{R}} \\ \subsetneq & T_pY_3 \cap T_pZ = \langle (1, -1, 0), (1, 1, 0) \rangle_{\mathbb{R}} = T_pZ. \end{aligned}$$

Then $Y_1 \cap Z$ is clean and $Y_3 \cap Z$ is not clean.

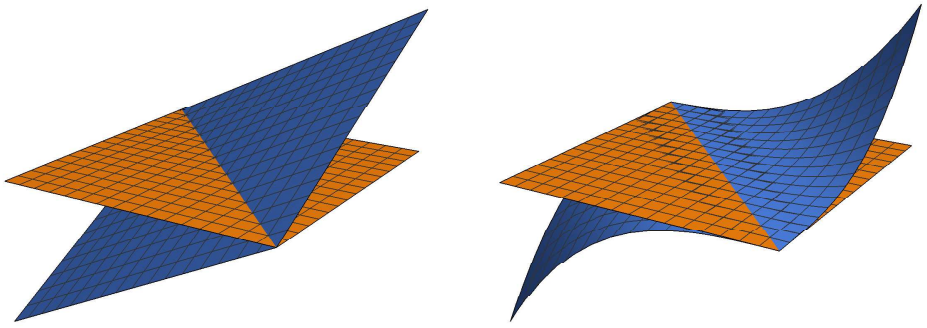

Figure 15. Clean intersection $Y_1 \cap Z$ and unclean intersection $Y_3 \cap Z$

In case of the clean intersection $Y_1 \cap Z$, we can pick up local coordinates (s, t, u) such as

$$s \begin{bmatrix} 1 \\ 1 \\ 0 \end{bmatrix} + t \begin{bmatrix} 1 \\ -1 \\ 0 \end{bmatrix} + u \begin{bmatrix} 1 \\ 1 \\ 2 \end{bmatrix}$$

near $Y_1 \cap Z$. Moreover $Y_1 \cap Z$ is transversal intersection since

$$\operatorname{codim}(Y_1) + \operatorname{codim}(Z) - \operatorname{codim}(Y_1 \cap Z) = 1 + 1 - 2 = 0.$$

In case of $Y_3 \cap Z$ we cannot choose appropriate local coordinates near $Y_3 \cap Z$.

In the proof of Theorem 7 we need to consider a product of the form

$$(\mathcal{R}_d \chi_D)^2 = \sum_{j=1}^{J} (\mathcal{R}_d \chi_{D_j})^2 + 2 \sum_{1 \leqq j < k \leqq J} \mathcal{R}_d \chi_{D_j} \cdot \mathcal{R}_d \chi_{D_k}.$$

In particular we shall investigate the interaction of conic Lagrangian submanifolds in $T^*G(d,n) \setminus 0$ of the form

$$\Lambda'_\phi \circ N^* \Sigma_j = \left\{ \left(\sigma, y - \pi_\sigma y;\ \eta(\cdots, 1)\right) :\ (y,\eta) \in N^* \Sigma_j, \sigma \in G_{d,n} \cap \eta^\perp \right\}.$$

We shall understand the structure of this conic Lagrangian submanifold. So we define two subsets of $G(d,n)$ as

$$S_j := \pi_{G(d,n)}(\Lambda'_\phi \circ N^* \Sigma_j) = \{(\sigma, y - \pi_\sigma y) : y \in \Sigma_j, \sigma \in G_{d,n} \cap T_y \Sigma_j\},$$
$$S_{jk} := S_j \cap S_k.$$

Then we have

Lemma 9.

- $\operatorname{codim} S_j = 1$, *and* $N^* S_j = \Lambda'_\phi \circ N^* \Sigma_j$.
- *If* $j \neq k$ *and* $S_j \cap S_k \neq \emptyset$, *then* S_j *intersects* S_k *transversely, that is,*

$$N^*_{(\sigma,x'')} S_j \cap N^*_{(\sigma,x'')} S_k = \{0\}$$

for any $(\sigma, x'') \in S_j \cap S_k$.

Here we observe an example of transverse intersection of $S_1 \cap S_2$ in $G(1,2)$. We set D_1 and D_2 in $\mathbb{R}^2$ as

$$D_1 = \{x^2 + y^2 < 1\}, \quad D_2 = \{(x-5)^2 + y^2 < 4\}.$$

Then we have

$$S_1 = \{(\theta, \pm 1) : \theta \in [0, \pi]\}, \quad S_2 = \{(\theta, 2 \pm 5\cos\theta) : \theta \in [0, \pi]\}.$$

We draw the intersection $S_1 \cap S_1$.

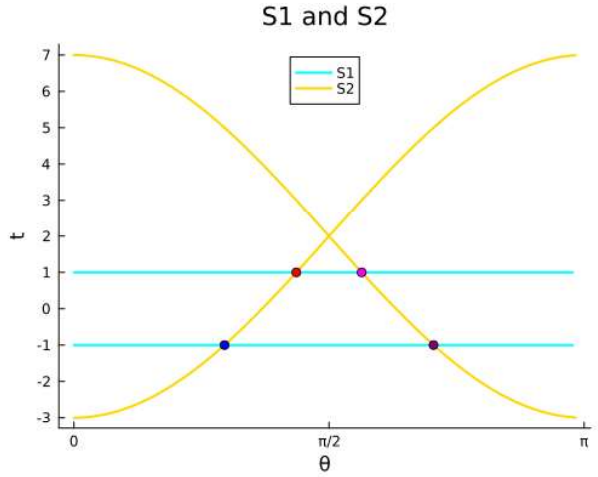

Figure 16. Transverse intersection S_1 and S_2 in $G(1,2)$

In the two-dimensional case $n = 2$, each intersecting point corresponds to a common tangential line, and the normal directions, which are singular directions, at tangent points are the same.

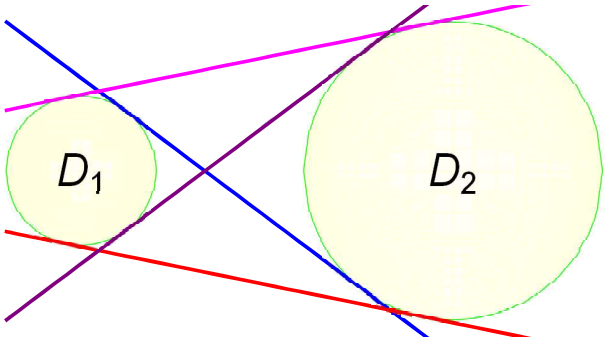

Figure 17. Common tangential lines corresponding to points in $S_1 \cap S_2$

In the higher dimensional case $n \geqq 3$, the set of pairs with a common tangent line becomes a connected $(n-2)$-dimensional submanifold $\mathcal{M}_{jk}^{(\pm)}$ of $\Sigma_j \times \Sigma_k$, and the singular directions at tangent points are not necessarily same. We now clarify this. For this purpose we introduce the projection of $\mathcal{M}_{jk}^{(\pm)}$ to Σ_j by

$$B_{jk}^{(\pm)} := \{y_j \in \Sigma_j \mid \exists y_k \in \Sigma_k \ \text{ s.t. } (y_j, y_k) \in \mathcal{M}_{jk}^{(\pm)}\},$$

which is an $(n-2)$-dimensional submanifold of Σ_j. Let Ω_{jk} be the connected subdomain of Σ_j enclosed by $B_{jk}^{(+)} \cup B_{jk}^{(-)}$.

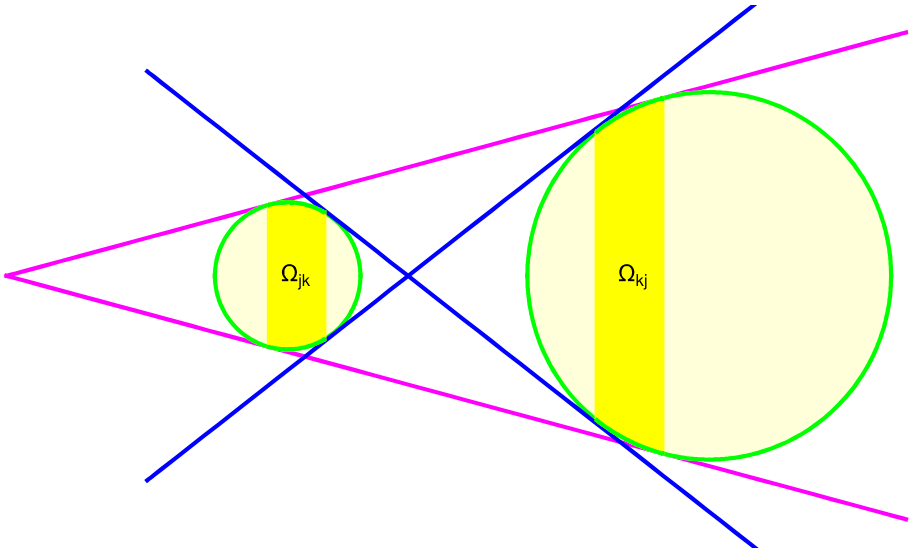

Figure 18. $\mathcal{L}_{jk}^{(+)}$, $\mathcal{L}_{jk}^{(-)}$, Ω_{jk} and Ω_{kj}

For any $y_j \in \Omega_{jk}$, there are many $y_k \in \Omega_{kj}$ such that Σ_j and Σ_k have common tangential line passing through y_j and y_k, but the normal directions at the points are different. We classify these two types of common tangent lines. Lemma 9 implies that $\operatorname{codim} S_{jk} = 2$. If $(\sigma, x'') \in S_{jk}$, then there exist $y_j \in \Sigma_j$ and $y_k \in \Sigma_k$ such that $\sigma \subset T_{y_j}\Sigma_j \cap T_{y_k}\Sigma_k$ and $x'' = y_j - \pi_\sigma y_j = y_k - \pi_\sigma y_k$. S_{jk} is a disjoint union of

$$S_{jk}^{(1)} = \{(\sigma, x'') \in S_{jk} : N_{y_j}^*\Sigma = N_{y_k}^*\Sigma\}, \quad S_{jk}^{(2)} = \{(\sigma, x'') \in S_{jk} : N_{y_j}^*\Sigma \neq N_{y_k}^*\Sigma\}.$$

we have the following.

Lemma 10. *We have clean intersections*

$$\begin{aligned}
(\Lambda'_\phi)^*\circ N^*S_j &= N^*\Sigma_j \setminus 0, \\
(\Lambda'_\phi)^*\circ N^*S^{(1)}_{jk} &= N^*\mathcal{L}_{jk} \setminus 0, && e = d(n-d-1), \\
(\Lambda'_\phi)^*\circ N^*S^{(2)}_{jk} &= (N^*\Omega_{jk} \setminus 0) \cup (N^*\Omega_{kj} \setminus 0), && e = d(n-d-2).
\end{aligned}$$

Lemma 10 says that $S^{(1)}_{jk}$ creates conormal singularities on $\mathcal{L}$, and $S^{(2)}_{jk}$ does not create additional singularities other than $N^*\Sigma$. This corresponds to the facts explained by Figures 12 and 13.

5.2 Paired Lagrangian distributions

We introduce paired Lagrangian distributions originated by [16].

Definition 11 (Paired Lagrangian distributions)**.** Let $\mu, \nu \in \mathbb{R}$. Suppose that Λ_0 and Λ_1 are cleanly intersecting conic Lagrangian submanifolds of $T^*X \setminus 0$, that is,

$$T_{(x,\xi)}\Lambda_0 \cap T_{(x,\xi)}\Lambda_1 = T_{(x,\xi)}(\Lambda_0 \cap \Lambda_1), \quad \forall (x,\xi) \in \Lambda_0 \cap \Lambda_1.$$

We say that $u \in \mathscr{D}'(X)$ belongs to $I^{\mu,\nu}(X; \Lambda_0, \Lambda_1)$ if $\mathrm{WF}(u) \subset \Lambda_0 \cup \Lambda_1$, and away from $\Lambda_0 \cap \Lambda_1$, we have $u \in I^{\mu+\nu}(X; \Lambda_0 \setminus \Lambda_1)$ and $u \in I^{\mu}(X; \Lambda_1)$.

We apply the next lemma to the product $\mathcal{R}_d\chi_{D_j} \cdot \mathcal{R}_d\chi_{D_k}$

Lemma 12 (Greenleaf-Uhlmann, 1993)**.** *Let X be an N-dimensional manifold, and let Y and Z be transversely intersecting submanifolds of X. We define integers k_1, k_2, l_1, and l_2 by*

$$\operatorname{codim} Y = k_1, \quad \operatorname{codim} Z = l_1, \quad \operatorname{codim} Y \cap Z = k_1 + k_2 = l_1 + l_2.$$

Then we have

$$\begin{aligned}
&I^{\mu+k_1/2-N/4}(X; N^*Y) \cdot I^{\nu+k_1/2-N/4}(X; N^*Z) \\
\subset &I^{\mu+k_1/2-N/4,\nu+k_2/2}(X; N^*(Y\cap Z), N^*Y) + I^{\nu+l_1/2-N/4,\mu+l_2/2}(X; N^*(Y\cap Z), N^*Z).
\end{aligned}$$

The transversality $N^*Y \cap N^*Z = \{0\}$ guarantees that the product can be well-defined since

$$\xi + \eta \neq 0 \quad \text{for} \quad \xi \in N^*_xY, \quad \eta \in N^*_xZ, \quad x \in Y \cap Z.$$

5.3 Overview of the proof of Theorem 7

Set

$$\mathscr{A} := \sum_{j\neq k} I^{-(d+1)/2-N(d,n)/4,-(d+1)/2}\big(G(d,n); N^*S_{jk}, N^*S_j\big).$$

We remark that

$$\chi_{D_j} \in I^{-1/2-n/4}(\mathbb{R}^n; N^*\Sigma_j), \quad \mathcal{R}_d\chi_{D_j} \in I^{-(d+1)/2-N(d,n)/4}\big(G(d,n); N^*S_j\big) \subset \mathscr{A}.$$

We prove Theorem 7 in the following three steps.

- Lemma 12 proves that $(\mathcal{R}_d\chi_D)^2 \in \mathscr{A}$.
- It follows that $\mathscr{A}$ is an algebra. In particular

$$P_{MA} := \sum_{k=1}^{\infty} A_k(\alpha\varepsilon)^{2k}(\mathcal{R}_d\chi_D)^{2k} \in \mathscr{A}.$$

- Applying Lemmas 10, 13, and 14 to P_{MA}, we prove Theorem 7.

We state Lemmas 13 and 14.

Lemma 13. *$\mathcal{R}_d^*(-\Delta_{x''})^{d/2}$ is a Fourier integral operator of order*

$$\frac{d}{2} + \frac{N(d,n)}{4} - \frac{n}{4}$$

with a canonical relation

$$(\Lambda'_\phi)^* := \{(x,y,\xi,\eta) : (y,x,;\eta,\xi) \in \Lambda'_\phi\}.$$

Lemma 14 ([14, Theorem 25.2.3])**.** *Assume the following conditions.*

- *A_1 and A_2 are Lagrangian distributions such as*

$$A_1 \in I^{m_1}(X\times Y, C_1), \quad A_2 \in I^{m_2}(Y\times Z, C_2),$$

  and are properly supported.

- *The intersection $C' := C'_1 \circ C'_2$ is proper, connected, and clean with excess e, that is, $C'_1 \times C'_2$ cleanly intersect*

$$T^*X \times \operatorname{diag}\big(T^*Y \times T^*Y\big) \times T^*Z$$

  with excess e.

Then

$$A_1 \circ A_2 \in I^{m_1+m_2+e/2}(X\times Z, C).$$

Finally we show how the clean intersection condition works in our analysis briefly. Basically we make use this condition to pick up appropriate local coordinates. If

$$u \in I^{-(d+1)/2-N(d,b)/4,-(d+1)/2}\big(G(d,n); N^*S_{jk}, N^*S_j\big),$$

then we can choose local coordinates $(x,y,z) \in \mathbb{R}\times\mathbb{R}\times\mathbb{R}^{N(d,n)-2}$ and find an amplitude $a(x,y,z,\xi,\eta)$ such that $S_j = \{x=0\}$, $S_{jk} = \{x=y=0\}$,

$$\partial^\gamma_{x,y,z}\partial^\alpha_\xi\partial^\beta_\eta a(x,y,z,\xi,\eta) = \mathcal{O}(\langle\xi;\eta\rangle^{-(d+2)/2-\alpha}\langle\eta\rangle^{-(d+2)/2-\beta}),$$

$$u(x,y,z) = \iint_{\mathbb{R}^2} e^{i(x\xi+y\eta)}a(x,y,z,\xi,\eta)d\xi d\eta$$

near $(x,y,z)=0$. Using formulas like this, we can obtain

$$\Big(I^{\mu,\nu}\big(G(d,n); N^*S_{jk}, N^*S_j\big)\Big)^2 \subset \mathscr{A},$$
$$I^{\mu,\nu}\big(G(d,n); N^*S_{jk}, N^*S_j\big)\cdot I^{\mu,\nu}\big(G(d,n); N^*S_{jk}, N^*S_k\big) \subset \mathscr{A}.$$

References

[1] H. Andrade-Loarca, G. Kutyniok, O. Öktem, and P. C. Petersen, *Extraction of digital wavefront sets using applied harmonic analysis and deep neural network*, SIAM Journal on Imaging Sciences, **12** (2019), pp.1936–1966.

[2] T. A. Bubba, G. Kutyniok, M. Lassas, M. Marz, W. Samek, S. Siltanen, and V. Srinivasan, *Learning the invisible: a hybrid deep learning-shearlet framework for limited angle computed tomography*, Inverse Problems, **35** (2019), 064002.

[3] H. Chihara, *Microlocal analysis of d-plane transform on the Euclidean space*, SIAM J. Math. Anal., **54** (2022), pp.6254–6287.

[4] J. J. Duistermaat, "Fourier Integral Operators", Birkhäuser, Boston, 1995.

[5] C. L. Epstein, "Introduction to the Mathematics of Medical Imaging, Second Edition", SIAM, Philadelphia, 2008.

[6] A. Greenleaf and G. Uhlmann, *Recovering singularities of a potential from singularities of scattering data*, Comm. Math. Phys., **157** (1993), pp.549–572.

[7] A. Grigis and J. Sjöstrand, "Microlocal Analysis for Differential Operators: An Introduction", Cambridge University Press, Cambridge, 1994.

[8] V. Guillemin and S. Sternberg, "Geometric Asymptotics", Mathematical Surveys, **14**, American Mathematical Society, Providence, RI, 1977.

[9] V. Guillemin and G. Uhlmann, *Oscillatory integrals with singular symbols*, Duke Math. J., **48** (1981), pp.251–267.

[10] S. Helgason, "Integral Geometry and Radon Transforms", Springer-Verlag, New York, NY, 2011.

[11] L. Hörmander, "The Analysis of Linear Partial Differential Operators I", Springer-Verlag, Berlin, 1983.

[12] L. Hörmander, "The Analysis of Linear Partial Differential Operators II", Springer-Verlag, Berlin, 1983.

[13] L. Hörmander, "The Analysis of Linear Partial Differential Operators III", Springer-Verlag, Berlin, 1985.

[14] L. Hörmander, "The Analysis of Linear Partial Differential Operators IV", Springer-Verlag, Berlin, 1985.

[15] V. P. Krishnan and E. T. Quinto, *Microlocal analysis in tomography*, Handbook of mathematical methods in imaging, Vol. 1, 2, 3, pp.847–902, Springer-Verlag, New York, 2015.

[16] R. Melrose and G. Uhlmann, *Lagrangian intersection and the Cauchy problem*, Comm. Pure Appl. Math., **32** (1979), pp.483–519.

[17] B. Palacios, G. Uhlmann and Y. Wang, *Quantitative analysis of metal artifacts in X-ray tomography*, SIAM J. Math. Anal., **50** (2018), pp.4914–4936.

[18] H. S. Park, J. K. Choi and J. K. Seo, *Characterization of metal artifacts in X-ray computed tomography*, Comm. Pure Appl. Math., **70** (2017), pp.2191–2217.

[19] E. T. Quinto, *Singularities of the X-Ray transform and limited data tomography in* $\mathbb{R}^2$ *and* $\mathbb{R}^3$, SIAM J. Math. Anal., **24** (1993), pp.1215–1225.

[20] E. T. Quinto, *An introduction to X-ray tomography and Radon transforms*, "The Radon Transform, Inverse Problems, and Tomography", Proceedings of Symposia in Applied Mathematics, **63**, pp.1–23, American Mathematical Society, Providence, RI, 2006.

[21] Y. Wang and Y. Zou, *Streak artifacts from nonconvex metal objects in X-ray tomography*, Pure Appl. Anal., **3** (2021), pp.295–318.

HIROYUKI CHIHARA
Colloge of Education
University of the Ryukyus
Nishihara, 903-0213 Okinawa, Japan
hc@trevally.net